

Impacts of Juniper Vegetation and Karst Geology on Subsurface Flow Processes in the Edwards Plateau, Texas

Surajit Dasgupta, Binayak P. Mohanty,* and J. Maximilian Köhne

ABSTRACT

Impacts of Ashe juniper (*Juniperus ashei* J. Buchholz) and karst geology on the regional water cycle in the Edwards plateau region of Texas are complex and not well understood. The objective of our study was to gain a comprehensive understanding of the subsurface flow processes occurring at a juniper woodland site on the Edwards Plateau near Honey Creek State Natural Area. A 2.3-m-deep, 7-m-long trench was excavated at the downslope end of a 7 by 14 m experimental plot, and time domain reflectometry (TDR) probes were installed at various locations within the trench face to measure volumetric water contents. A multi-port telescopic boom type rainfall simulator was used to provide artificial rainfall on the plot. Six rainfall simulations and two dye-tracer tests were conducted on the plot during a 7-mo period. Subsurface flow was visually inspected at various locations on the trench face during artificial rainfall experiments and water content was monitored near slow and fast flow regions using TDR probes. The total volume of subsurface flow was also recorded after each rainfall simulation event. Results demonstrated that subsurface flow occurred in a bimodal manner, consisting of preferential/macropore flow around juniper root channels and planar fractures in the limestone, and pseudo-matrix flow through the soil matrix (water flowing primarily through the intermediate layers and lenses of soil between the rock layers). Preferential/macropore flow at the trench face depended on imposed boundary conditions and was independent of antecedent moisture content in the soil matrix. Pseudo-matrix flow response time decreased with high rainfall. During large rainfall events (>200 mm), water exchange was observed between the fractures and soil matrix. No apparent water exchange occurred between fractures and the soil matrix during small rainfall events. The dye studies indicated that fractures and juniper root channels are primary pathways for preferential/macropore flow occurring within the plot.

REGIONAL ECOHYDROLOGY of Edwards aquifer and plateau region in Texas has been affected by historical encroachment of invasive plant species such as Ashe juniper (Archer, 1994; Wilcox, 2002) and underlying karst geology. To achieve a sustainable water resource management, it is imperative to gain a proper understanding of the hydrogeologic and ecohydrologic processes occurring in this region. From the ecohydrologic perspective, an important issue is to gain a comprehensive insight into the role played by plants in the water cycle. Ashe juniper is by far the most dominant species of trees found within the Edwards aquifer region.

Studies related to juniper and surface water (overland flow) present inconsistent results. Based on a compari-

son between treated and untreated juniper plots in the Edwards region, Dugas et al. (1998) stated that juniper removal had no consistent effect on overland flow generation. Richardson et al. (1979) found that root plowing to remove junipers in the Edwards plateau reduced overland flow by 20%. Plowing increased water storage in depressions within the watershed, which either infiltrated through the rock fractures or evaporated. However, they also found that killing mesquite trees in the Blackland Prairie region of Texas by chemical treatment reduced evapotranspiration (ET) and subsequently increased surface runoff by 10%. Wright et al. (1976) found that overland flow increased in the period ranging between 2 and 3 yr after the removal of junipers by burning. This was probably due to the fact that during the initial years following tree removal, there was less infiltration and ET. Wilcox (2002) suggested that in karst regions of Texas, there is a possibility of juniper removal resulting in increased streamflow. The presence of juniper trees causes water to infiltrate the soil surface and move rapidly through the root zone (network) as preferential flow. Newman et al. (1998, 2004) documented that lateral subsurface flow occurs mainly from root macropores. Their hypothesis from preferential flow studies in a semiarid ponderosa pine hillslope suggested that root structures, which are active agents of lateral subsurface flow, create a saturated halo with time, and this eventually forms a perched water table. It seems evident from the past studies that more detailed experiments need to be conducted in such areas to facilitate our understanding of juniper–water interactions.

In addition to ecohydrological controls, the hydrogeologic characteristics of the underlying aquifer play a vital role in determining the hydrology of the Edwards region. Karstic aquifers are unique because, unlike other aquifers, they are characterized by a threefold porosity–permeability. Pore spaces formed within the rocks by constitutive minerals form the primary or matrix porosity (sub-millimeter scale), joints and fractures produced by orogenic processes form the secondary or fracture porosity (millimeter scale), and the cavities and integrated conduits produced by chemical dissolution, which are a characteristic feature of karst regions, form the tertiary or conduit porosity (centimeter to meter scale) (White, 1998). Thus, a sound knowledge of the hydrology of such triple porosity–permeability media entails an understanding of the rate of recharge into and through the various porosity components and the exchange of water between these components (White, 2002).

Several studies have been conducted to investigate preferential flow processes in the vadose zone using fluorescent dyes (Flury et al., 1994; McKay et al., 1993;

S. Dasgupta, B.P. Mohanty, and J.M. Köhne, Dep. of Biological and Agric. Engineering, 2117 TAMU, Texas A & M Univ., College Station, TX 77843-2117. J. Maximilian Köhne now at Univ. of Rostock, Germany. Received 12 June 2005. *Corresponding author (bmohanty@tamu.edu).

Published in Vadose Zone Journal 5:1076–1085 (2006).

Original Research
doi:10.2136/vzj2005.0073

© Soil Science Society of America
677 S. Segoe Rd., Madison, WI 53711 USA

Abbreviations: ET, evapotranspiration; TDR, time domain reflectometry.

Jardine et al., 1999). These organic dyes are primarily used because they are cheap, easy to handle, and nontoxic (Käss, 1998). Flury et al. (1994) suggested that the initial moisture content has no effect on the penetrating depth of macropore flow in their experiments conducted on structured and nonstructured soils in Switzerland. In field experiments, McKay et al. (1993) compared the flow rates between nonreactive tracers and bacteriophage tracers in highly fractured, clay-rich glacial till plains in Canada and found that the latter were several orders of magnitudes higher than the former. Experimental analysis and modeling results conducted by Jardine et al. (1999) by injecting tracers in fractured shale bedrock in Tennessee showed that flow occurred as a combination of fracture and matrix flow. The above-mentioned studies mainly focus on the physical properties of dyes and tracers (advection–diffusion, sorption and/or dispersion) and investigate breakthrough curves of such dyes and tracers after they were applied either in laboratory conditions, field sites, and/or models. The breakthrough curves provide answers to the processes and mechanisms of macropore/preferential flow occurring in the study domains. Mortensen et al. (2004) pointed out that while most such studies have been conducted in saturated conditions (McKay et al., 1999; Sidle et al., 1998), very few (Forrer et al., 1999) have been conducted in unsaturated conditions.

We report results of an experiment on a field plot in the Edwards plateau of Texas dominated by juniper vegetation and karst geology. Subsurface flow processes and patterns were monitored and investigated by artificially simulating a series of rainfall events of different

intensities on the plot. Since the primary focus of our study was to determine the impact of juniper vegetation and karst geology on the local hydrology, we decided to limit the scope of the tracer studies as a supplemental tool to assist in our understanding of the flow processes in the study region. Thus, we present the arrival times and peak flow times of dyes that were used during the experiment without delving into detailed analysis of dye tracer breakthrough curves. Thus, the primary objectives of this study were to: (i) obtain an improved understanding of the nature and origin of subsurface flow processes occurring in a juniper dominated plot with underlying karst geology and (ii) analyze the effects of initial and surface boundary conditions on the onset, rate, and spatiotemporal patterns of subsurface flow.

MATERIALS AND METHODS

Site Description

The study area is located within the 9-km² Honey Creek State Natural Area (29°44' N, 98°26' W), which is part of the Guadalupe River State Park, located in the western part of Comal County, Texas (Fig. 1). The climate is classified as subhumid, subtropical, with mean annual rainfall of approximately 800 mm (Kuniansky et al., 2001). Our experimental plot (Fig. 2) is 14 by 7 m in size, with a land surface slope of about 1%. The ground surface was characterized by a black-colored litter and organic soil layer. Ash juniper and live oak were the most dominant species around the plot along with occasional patches of cacti. The surface topography of the plot was characterized by several mild depressions 10 to 20 cm deep and a few meters in diameter. The plot contained nine juniper trees with variable basal diameters ranging from 0.05 to 0.56 m.

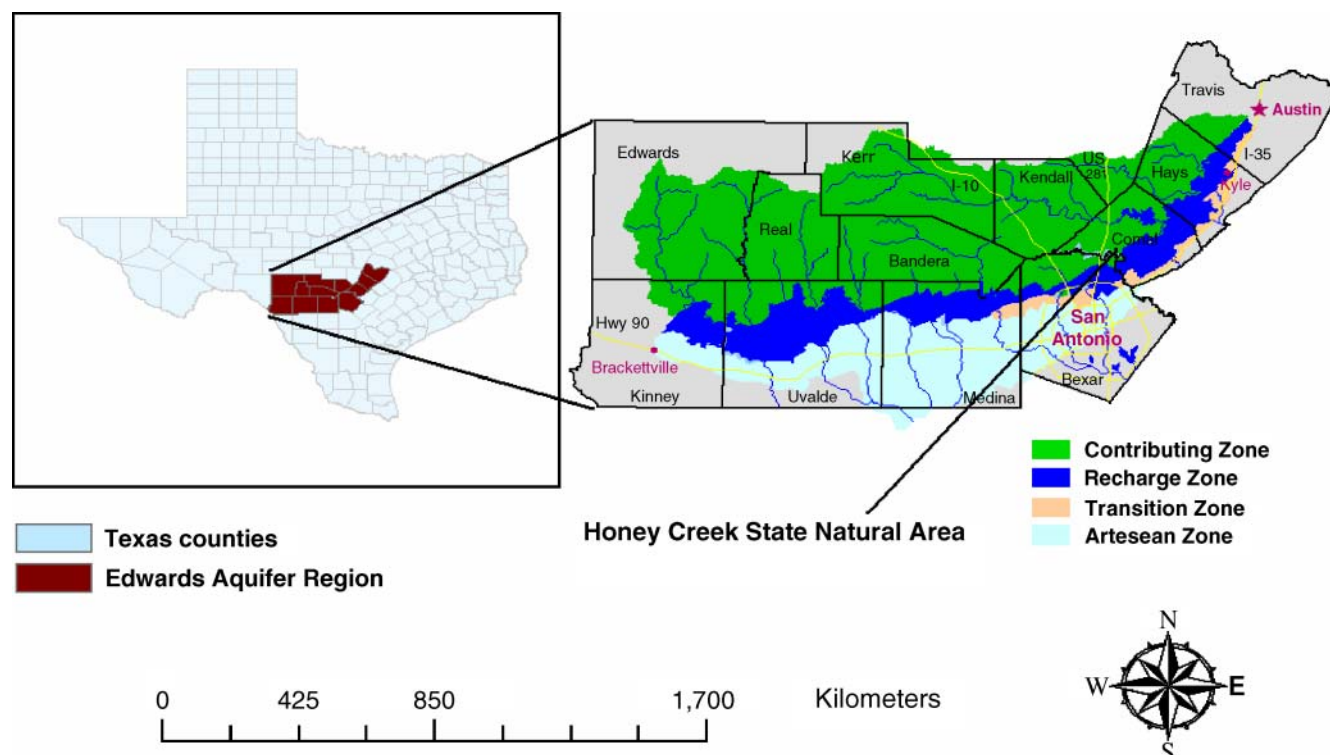


Fig. 1. The study area was the Honey Creek State Natural Area located in Comal County TX. Also shown are the various hydrologic zones of the Edwards aquifer.

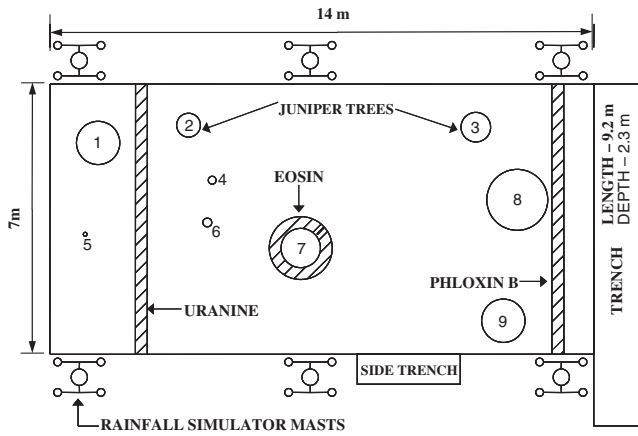


Fig. 2. Honey creek experimental plot with spatial locations of juniper trees, rainfall simulator masts, and the trench. Application bands of three dyes (Uranine, Phloxin-B, and Eosin) during dye-tracer studies are also illustrated in the layout.

A trench (9.2 m long, 2.3 m deep) was excavated using a backhoe at the downslope end of the plot for monitoring the subsurface flow processes occurring below the plot in the karstic vadose zone. At the trench face (Fig. 3), the soil-rock profile consists of parallel geologic layers (reflecting flow regions) that were assumed to be representative of the whole plot. A schematic diagram of the trench cross section is shown in Fig. 4. The spatial locations of 12 TDR probes that were used to determine the volumetric water contents are also shown in Fig. 4. Note that a representative fraction of 4.5 m of the total length of 9.2 m of the trench face has been illustrated.

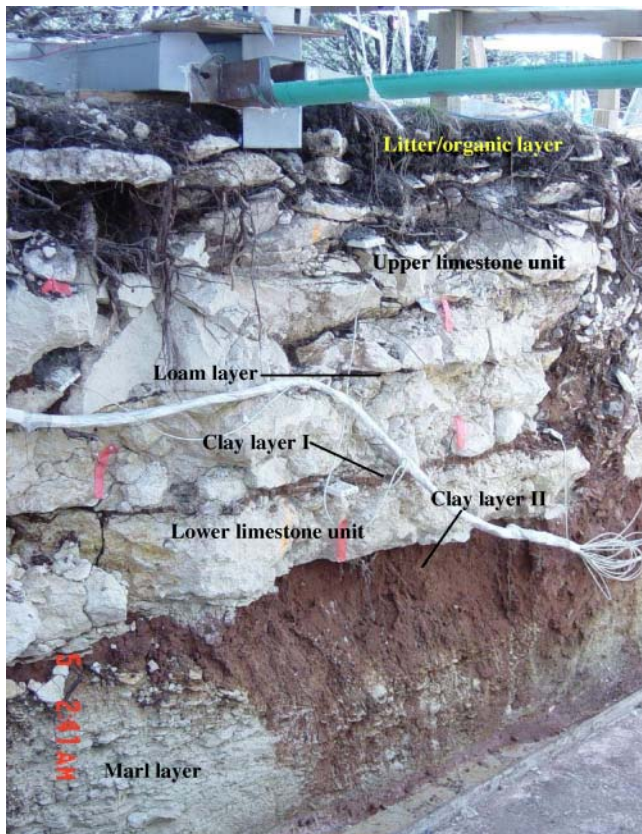
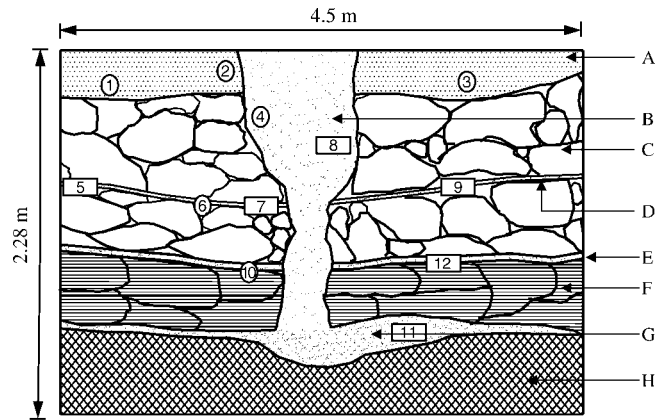
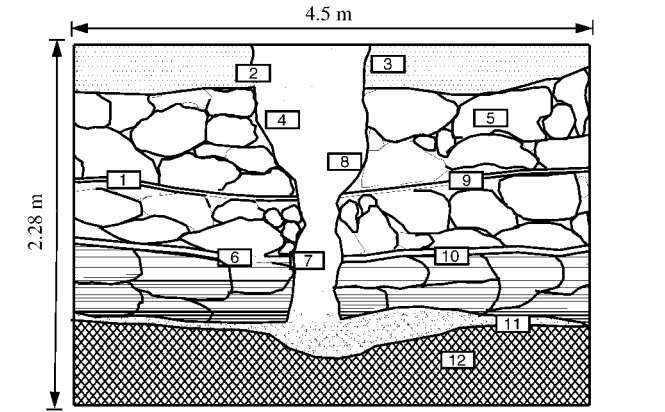


Fig. 3. Photograph showing cross section of trench face beside the plot.



(a)



(b)

A - Litter/organic layer	E - Clay layer I
B - Silty clay wedge	F - Lower limestone unit
C - Upper limestone unit	G - Clay layer II
D - Loam layer	H - Marl layer

Fig. 4. Schematic sketch of trench cross-section illustrating the stratification of the trench face. (a) The older TDR probe locations (October to mid December 2003, Simulation Runs 1-5); (b) newer locations (mid December 2003 to May 2004, Simulation Runs 6 and dye tests). The older TDR probes are represented by circles, while the newer ones are represented by rectangles.

Additionally, a small and shallow (1 m long, 1 m deep) side trench (Fig. 2) was dug for examining the presence of any shallow subsurface flow, perpendicular to the direction of the land surface slope.

The topmost horizon (Fig. 4) of the trench at the study site was divided into two layers. The upper (litter) layer (0.04–0.1 m) was composed of humus and undecomposed and live roots. The lower layer was characterized by an organic rich black clay. The upper limestone unit (0.38–0.56 m thick) was characterized by a large layer of limestone intersected by horizontal and vertical fractures. A thin (0.01–0.04 m thick) loam fracture fill (33% sand, 47% silt, and 20% clay) cut across the upper limestone unit. The first clay fracture fill (13% sand, 36% silt, and 51% clay) extended across the trench face in between the two (upper and lower) limestone units and had variable thickness (0.03 and 0.07 m) and contained some amount of live roots. The lower limestone unit (0.4–0.46 m) was less fractured than the upper limestone unit. The second clay fracture fill (8% sand, 34% silt, and 58% clay) with live roots, located below the lower limestone unit, was a thin strip (0.05 m) with a maximum thickness of 0.50 m at the center of the trench. The silty-clay (11% sand, 44% silt, and 45% clay) wedge existed as a vertical strip of fracture fill soil that ran

from the upper litter layer to the second clay layer. The soil samples from the trench face were analyzed by the (ASTM, 1961) texture analysis method in the Texas A&M University soil hydrology laboratory. The “marl” layer that was found as the lowermost horizon of the trench was a clay-rich limestone zone whose thickness varied from 1.02 m at the extreme left to 0.63 m at the extreme right portion of the trench.

Rainfall Simulation and Data Collection

A rainfall simulator system was installed to provide artificial rainfall on the plot. It consisted of six telescopic masts of 15-m height. Three masts were set up on either side along the length of the plot (Fig. 2). Each mast had four sprinkler heads individually controlled by manually operated valves. The masts were connected via a pump (Honda WP20X, American Honda Power Equipment Division, Alpharetta, GA), flow meter, and pressure gauge to a 18 927-L (5000 gallon) collapsible water tank. The simulator was capable of delivering rainfall intensities varying from 25.4 to 152.4 mm h⁻¹. Eight different rainfall simulations were performed at the site between October 2003 and May 2004. The surface components of the water budget were monitored as follows. First, rainfall was measured using spatially distributed rain gauges placed inside and outside the plot. Second throughfall (rainfall minus interception) was measured using throughfall funnels placed beneath the juniper canopy inside the plot. Third, stemflow was measured using a stemflow collar around two (replicates) juniper trees that measured the amount of water that was funneled by the stems to the base of the tree trunk. Next, runoff was measured by a 150-mm H-flume placed at the downslope end of the plot. Finally, a sump was created within the trench to measure the total volume of subsurface flow using a sump pump and flow meter. Any direct rainfall input to the trench was prevented by constructing a plastic roof over the trench while the water loss to deep percolation through the trench floor was minimized by installing a concrete floor.

It was observed that, after each simulated rainfall event, subsurface seepage flow occurred at various point locations within the trench face. This was visually inspected during each rainfall simulation by manually recording the time of arrival (response time) of the three-dimensional flow at the trench face. Stop watches were used to determine the exact time of arrival (from the start of the rainfall event) when water started dripping from the trench face. At certain locations, we calculated the seepage flux by measuring the time it took to fill a known volume of a measuring beaker. Besides the manual flux measurement, the TDR 100 (Campbell Scientific, Logan, UT) probes were used to measure profile soil water contents within the trench. The 15-cm-long TDR probes were multiplexed and connected to a Campbell Scientific CR10-X data logger for continuous monitoring of soil water content at 10-min intervals for each rainfall simulation event. Twelve TDR probes were strategically placed at various locations within the trench face to record the arrival of the wetting front at each flow region (as shown in Fig. 4). Two additional probes (S1 at the 12-cm depth and S2 at the 45-cm depth) were placed within the trench dug at the side of the plot (Fig. 2). Note that the TDR probes could be located in the soil or rock matrix and clay-filled fractures excluding the larger voids and conduits.

Readings from each TDR probe were collected for each rainfall simulation event for 48 h, starting from the onset of the first run of a particular simulation event. This 48-h duration was determined after an initial data analysis revealed that the probes showed a rise in water contents after 23 to 30 h from the start of the rainfall event. The apparent dielectric readings obtained from the probes were converted to volumetric water

contents using the Topp et al. (1980) relationship. The volumetric water content values as obtained from the TDR probes were analyzed to determine characteristic hydraulic response time, as well as initial and final moisture contents for the various distinct flow regions (including fractures, fracture fills, juniper root zones) of the soil–rock system. Linear regressions were established between these hydraulic response parameters and the total rainfall amount for each simulation event. The initial moisture content was taken as the arithmetic mean of the values recorded by the probes for a period of 15 to 20 h before the probes registered a rise. The final moisture content was calculated by taking the arithmetic mean of the highest values recorded by the probes until the values started to decrease.

The first phase of data collection lasted from August to mid December in 2003. During the second phase (mid December 2003 to May 2004), some of the spatial locations of the probes within the trench face were altered to better monitor the flow processes (Fig. 4a and 4b). Spatial locations of the old and new positions of each TDR probe are provided in Table 1. Details of the rainfall simulation events are provided in Table 2. Each rainfall simulation consisted of either two or three separate runs interrupted by periods when no water was added to the plot. These interim periods were required to manually record the readings of all devices that measured the surface components of the water budget.

Consider any rainfall simulation event s ($s = 1, 2, 3, \dots, n$) consisting of j number of separate runs ($j = 1, 2, \dots, m$) and g number of interim periods ($g = 1, 2, \dots, p$). The average intensity (Table 2) for s was calculated as

$$I_s = \frac{\sum_{j=1}^m i_j d_j}{\sum_{j=1}^m d_j + \sum_{g=1}^p d_g} \quad [1]$$

where, I_s (mm) is the average rainfall intensity for simulation s , i_j (mm) is the intensity of the j th run, d_j (h) is duration of the j th run and d_g (h) is the duration of the g th no-addition interim period between the runs. The no-addition interim periods were assumed to have zero rainfall intensity.

Dye tracer experiments were conducted in addition to the rainfall simulation experiments to supplement our understanding of the subsurface flow processes, with special emphasis on their origin and the nature of the flow paths (matrix flow in soil–rock or preferential flow through root channels and/or geological fractures). Three different fluorescent dyes

Table 1. Spatial locations of the TDR probes before and after the adjustments were made. “Unit” indicates the flow region in which the probes were located; “Depth” indicates the depth of each probe from the top surface of the trench face.

Probe	Old location		New location	
	Unit	Depth	Unit	Depth
		m		m
1	Litter	0.25	Loam	0.61
2	Litter	0.15	Litter	0.40
3	Litter	0.22	Litter	0.22
	Upper limestone	0.48	Upper limestone	0.40
5	Loam	1.12	Upper limestone	0.43
6	Loam	1.14	Clay I	1.14
7	Loam	0.91	Clay I	1.06
	Upper limestone	0.68	Upper limestone	0.91
9	Loam	0.99	Loam	0.68
10	Clay I	1.78	Clay I	1.01
11	Clay II	2.17	Clay II	2.17
12	Clay I	1.44	Marl	2.35
S1	–	–	Litter	0.12
S2	–	–	Upper limestone	0.45

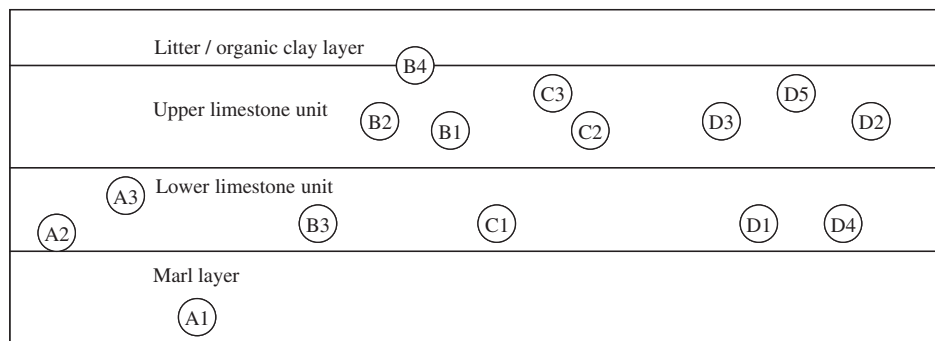
Table 2. Details of various rainfall simulation events carried out at the plot. Each simulation event contained a succession of runs with time gaps in between. The average intensity (Eq. [1]) and total rainfall amount for each simulation event were calculated.

Simulation	Date	Run	Intensity per run	Duration	Time gaps	Average Intensity	Total rainfall
			mm h ⁻¹	h	h	mm h ⁻¹	mm
Sim 1	3 Oct. 2003	1	59.20	2.00	1.00	43.9	170.2
		2	58.90	0.88			
Sim 2	17 Oct. 2003	3	8.70	3.50	1.00	7.0	56.4
		4	7.40	3.50			
Sim 3	31 Oct. 2003	5	12.40	3.50	1.20	9.9	74.2
		6	11.00	2.80			
Sim 4	5 Dec. 2003	7	59.00	1.00	2.48	24.0	107.6
		8	48.60	1.00			
Sim 5	11 Dec. 2003	9	67.50	0.75	1.083	21.0	108.9
		10	44.80	1.00	1.35		
		11	13.50	1.00			
Sim 6	18 Dec. 2003	12	91.20	0.75	1.45	24.8	134.1
		13	52.00	1.00	1.21		
		14	13.70	1.00			
Dye-test 1	30 Jan. 2004	15	25.40	4.00	1.23	40.8	254.0
		16	152.40	1.00			
Dye-test 2	13 May 2004	17	23.40	4.00	1.13	37.9	232.0
		18	138.45	1.00			

(Phloxin B, Eosin, and Uranine) were applied on three different locations (as illustrated in Fig. 2) within the plot to enable us to differentiate between various subsurface flow paths, such as network of root channels and interconnected fractures. Uranine was applied approximately 12 m from the trench face and Phloxin B was applied about 0.9 m from the trench face. Eosin was applied around the base of a centrally located juniper tree within the plot to characterize the origin of preferential flow (water) near the tree base because of funneling through root channels or fracture enhanced by root expansion. The dyes were dissolved in approximately 3.8 L (1 gallon) of deionized water and applied to the litter layer using a handheld garden sprayer. These dyes were chosen for their easily detectable fluorescent color and comparable absorption properties.

During the first dye-tracer test (30 Jan. 2004), all three dyes—Phloxin B (160 mg), Eosin (140 mg), and Uranine (40 mg)—were applied. After the application of the three dyes,

two rainfall simulation runs (15 and 16) were performed (Table 2). Water samples were then collected from 15 outflow (seepage) locations (Fig. 5) within the trench face at 10-min intervals. These samples were analyzed using a Spectrofluorometer (PerkinElmer, Wellesley, MA). The analysis of dye in the effluent water revealed that the applied dye concentrations used were too low for any clear spatiotemporal signature. Subsequently, a second dye-tracer experiment (13 May 2004) was conducted and the concentrations were increased for all three dyes—Phloxin B (1665 mg), Eosin (1500 mg), and Uranine (1000 mg). The dye application, location, and scheme of rainfall simulation for the second dye tracer test were kept similar to that of the first test. This approach also minimized the corruption of data in the second dye trace study due to any leftover dye from the first run. It is noteworthy that the sequences of outflow–seepage locations observed across the trench face (Fig. 5) for both the dye tracer tests were identical.



Sampling locations	Description
A1	In a hole in the lower marl layer
A2	Within the second fracture fill clay layer
A3	In a fracture within lower limestone unit
B1	In a fracture within upper limestone unit
B2	In a fracture within upper limestone unit
B3	Within the second fracture fill clay layer
B4	Within clay layer of upper litter/clay layer

Sampling locations	Description
C1	Within the second fracture fill clay layer
C2	Within the first fracture fill clay layer
C3	Within first fracture fill loam layer
D1	In a fracture within lower limestone unit
D2	Within the first fracture fill clay layer
D3	In a fracture within upper limestone unit
D4	In a fracture within lower limestone unit
D5	In a fracture within upper limestone unit

Fig. 5. Dye sampling and seepage points within the trench face.

RESULTS AND DISCUSSION

Subsurface seepage flow that was manually recorded at the trench face usually occurred within 3 to 5 h from the onset of each simulation run. This was assumed to be the fast component of the subsurface flow. The TDR probes usually took much longer (23–30 h) to respond. Thus, we noted that the probes predominantly recorded the slow component of the subsurface flow.

The subsurface seepage flow response times (during the two dye tracer studies) measured at various locations within the trench face are illustrated in Fig. 6. Rainfall simulation runs 15 and 17 (with intensities of 25.4 and 23.4 mm h⁻¹, respectively) resulted in outflow from only seven locations, whereas runs 16 and 18 (with intensities of 152.4 and 138.4 mm h⁻¹, respectively) resulted in outflow from 15 locations on the trench face. This demonstrated that a larger segment of the plot and its pore network contributed to the outflow at the trench face when the rainfall intensity was increased. Furthermore, the response times for low intensity runs (15 and 17) are much higher than those of the high intensity runs (16 and 18), revealing that outflow response times drastically reduced for high rainfall intensity. It also appears that the wetting front at the trench did not follow any specific horizontal or vertical progression. For example, during low intensity runs 15 and 17, seepage points B1 and C1 in the upper and lower limestone units appeared earlier than the other seepage points located at shallower depths. Similarly for the high intensity runs 16 and 18, seepage points A1 (in Marl layer) and C1 (in lower

limestone unit) appeared much faster than the other seepage points on the trench face. Also appearance of the slow reacting seepage points (e.g., D5) vary between the rainfall simulation runs.

A comparison of the sequence of wetting up of the seepage points between runs shows a (Pearson's ranked) sequence correlation coefficient of 0.78 for low intensity runs (15 and 17) and a sequence correlation of 0.81 for the high intensity runs (16 and 18). This signified that, based on the spatial locations of the seepage points within the trench face, the sequence of outflow was comparable for similar rainfall intensities. That is, there was a recurrent flow pattern along same flow paths characteristic for a particular rainfall intensity. The response times of the first appearance of dyes along with peak arrival times (numbers against bars) are shown in Fig. 7 during the second dye-tracer test. The response times are defined as the time from the onset of simulated rainfall until the moment when these dyes were first detected in the water samples collected during the test. The peak arrival time is the time passed between the onset of simulated rain and the maximum dye concentration in the water samples. For the two dyes, response times and peak arrival times at several locations were almost identical, even though Eosin was applied 7 m farther from the trench than Phloxin B. These findings suggest that dyes were not transported at constant spatially uniform velocity immediately after the onset of rain, since in that case the response and peak arrival times would have been related to the application distance from the trench. The

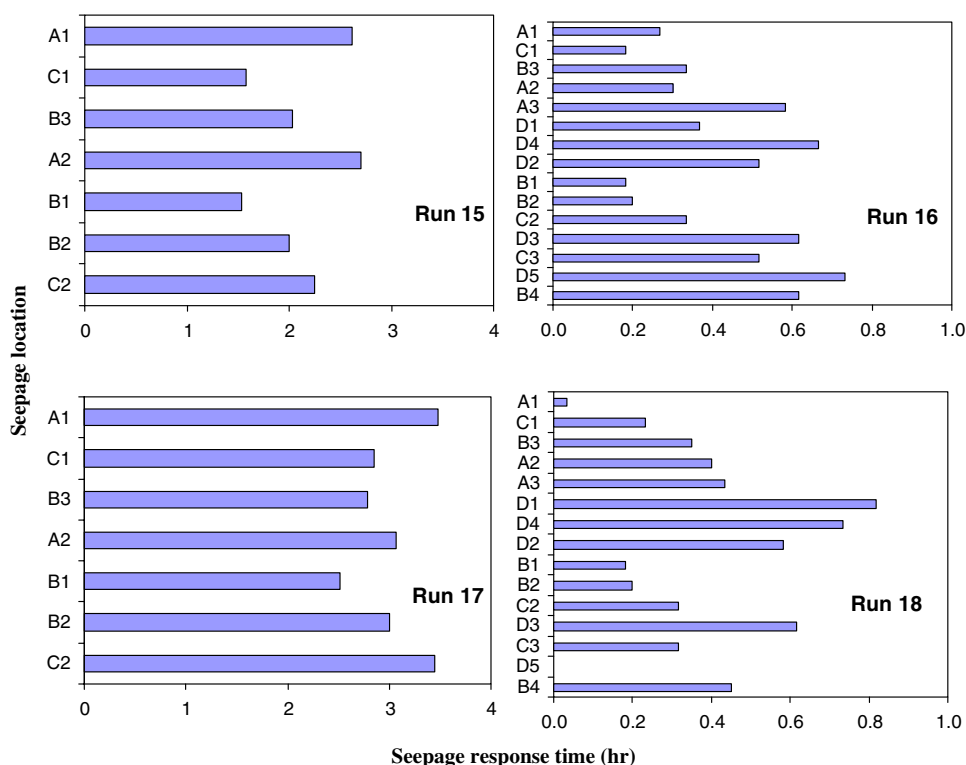


Fig. 6. Seepage response time indicates the initial onset of outflow from various seepage locations at the trench face. Refer to Fig. 5 for spatial locations for seepage points. Runs 15 and 17 were low intensity, long duration events. Runs 16 and 18 were high intensity, short duration events. Time of arrival was indistinguishable for low seepage volume at D5 for Run 18.

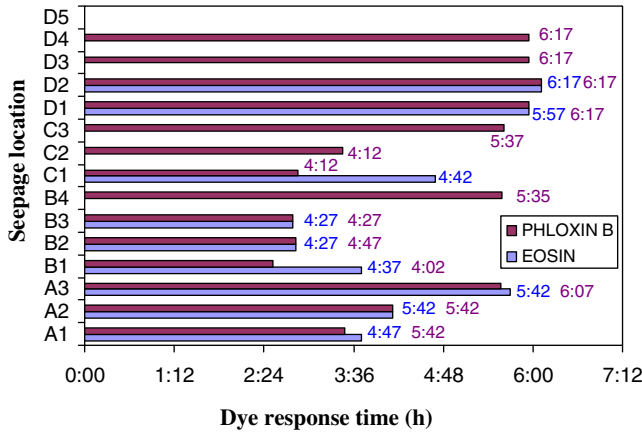


Fig. 7. Dye response times at various dye sampling locations within the trench face for the second dye-tracer test. Numbers beside the bars indicate peak concentration times as registered by the Spectrofluorophotometer.

results rather suggest that once flow paths became saturated and activated, dye transport must have occurred rapidly along similar preferential flow pathways, resulting in the simultaneous arrival of dyes from different application distances in the trench. At five seepage locations, only Phloxin B was observed, which could be because of the proximity of the application location of Phloxin B to the trench as compared with that of Eosin. Overall, these variations of fast flow and dye appearance, including their peak concentrations on the trench face, suggest that subsurface flow at the field site is dominated by various paths of interconnected roots and fractures–conduits.

On the basis of our findings, we suspect that some juniper roots preferentially grow along the geological fractures, while further widening these fractures with time, to extract water from the deeper layers as well as from large crevices and fissures within the limestone units. Past observational studies in the Edwards plateau region show juniper roots at depths of 10 to 15 m deep in underground caves hanging through their fractured roofs. This logic suggests that most of the subsurface flow seeped through the trench face may have entered the limestone units at the base of the juniper trees and follow the root–fracture network to reach the trench face.

Uranine (which was applied at the far end of the plot, with the largest concentration) did not appear at any of the 15 sampling locations of the trench face for the dye test. This suggests that perhaps seepage outflow at the trench face was dominated by flow processes occurring within the front half section of the plot, while Uranine may have been applied beyond the subsurface catchment area of the trench. Further investigation using a soaker hose study (by water input limited to the far end of the plot with no seepage appearing on the trench face) and subsurface fracture characterization using ground penetrating radar, GPR (results not presented here), confirmed a geological discontinuity between the two ends of the plot.

Typical TDR response times for a single rainfall simulation event (Sim 5) are illustrated in Fig. 8. Only five

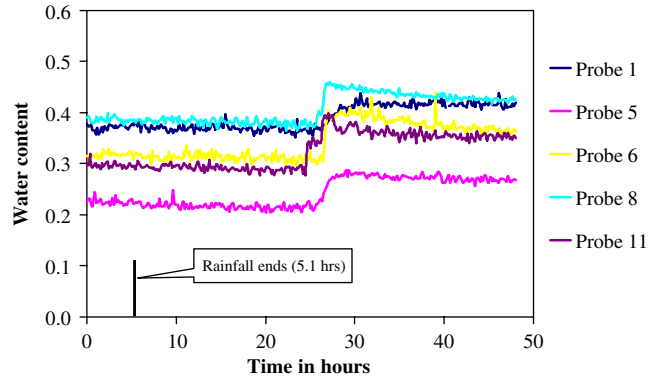


Fig. 8. Response times of various TDR probes for Simulation 5. (Total rainfall amount = 108.9 mm).

probes responded during this event, and the responses started about 25 h after the onset of the artificial rainfall simulation. The linear relationships of TDR response times with total rainfall and initial moisture content are shown in Fig. 9. The TDR response time was the time as registered by the TDR probe, which responded first to the arrival of the wetting front during a particular rainfall simulation event. Using a confidence limit of 95% ($\alpha = 0.05$), we observe a negative linear ($r^2 = 0.82$) relationship (significant at $\alpha = 0.05$) between rainfall amount (for eight different simulations) and response time, indicating that water reached the probes faster when the rainfall amount increased. In addition, a weak ($r^2 = 0.22$) relationship (significant at $\alpha = 0.05$) was found between response time and initial/antecedent moisture content. This is because the initial moisture content determined by TDR probes reflected the pseudo-matrix water (water that flows primarily through the intermediate layers and lenses of soil between the rock layers), while most flow occurred through fractures and conduits at the field site. This low correlation also uncovers the fact that in a juniper and karst dominated region, the fast flow is independent of antecedent conditions. The subsurface flow, however, depends on the

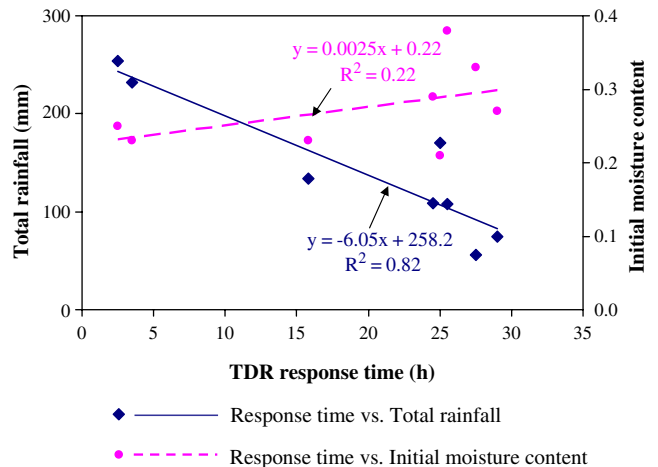


Fig. 9. Relationship of TDR response time with total rainfall and initial moisture content.

imposed surface boundary conditions. The initial and average response times registered by the TDR probes (Table 3) for the first six simulations fell within the 15- to 30-h range. It is noteworthy that, for the two-dye tracer tests (with high rainfall intensities), the TDR responses were much lower than the first four simulations. We hypothesize that when rainfall amount is large (>200 mm) water exchange occurs between the fast (rock and fracture) and slow (pseudo-matrix) flow domains resulting in faster TDR response time. This water exchange is probably driven by a pressure gradient effect (Köhne and Mohanty, 2005).

The total volume of rainfall that fell on the plot, and the total volume of subsurface flow measured for each rainfall simulation event are illustrated in Fig. 10. It is seen that subsurface flow volume generally tends to increase with increase in rainfall amount. However, discrepancy was observed during a high intensity rainfall simulation run (Dye 2), which we attribute to possible total rainfall loss due to wind drift (falling outside of the plot) and total seepage flow loss due to vertical and lateral deep recharge through other possible pathways that may have been inactive during the previous experiments because of antecedent hydrologic conditions at the site. Observed differences in the S1 TDR response (results not shown here) and accumulation of water on the side trench between the runs may reflect some of these behaviors at the experimental field site. Results of Simulation 3 were omitted from Fig. 10 due to lack of data.

During the rainfall simulation events, we observed that the rate of subsurface seepage flux varied at different locations of the trench face. At some places, it occurred as drips from small root tips (average discharge 0.00041 L s^{-1}), and at other locations the discharge was as high as 0.5 L s^{-1} . The high flow usually occurred at large fracture openings (>10-mm aperture) within the upper limestone layer. Since the seepage flux measurements were not made consistently during all rainfall simulation events except the two dye tracer studies, result statistics have not been presented in this study. Nevertheless, they provide a reasonable estimate of the nature and variability of the fast subsurface flow occurring at the trench face. The slow flow component usually occurred through the smaller fractures or pores (pseudo-matrix flow) present at the trench face and its onset usually lagged behind the fast flow component by

Table 3. Initial response times and average response times for all TDR probes for each simulation event.

Simulation	Total rainfall amount	TDR Probe Responses	
		Initial response time	Average response time
mm		h	
Sim 1	170.2	25.0	26.6
Sim 2	56.4	27.5	30.7
Sim 3	74.2	29.0	30.7
Sim 4	107.6	25.5	26.7
Sim 5	108.9	24.5	26.0
Sim 6	134.1	15.8	23.3
Dye-test 1	254.0	2.5	4.6
Dye-test 2	232.0	3.5	5.1

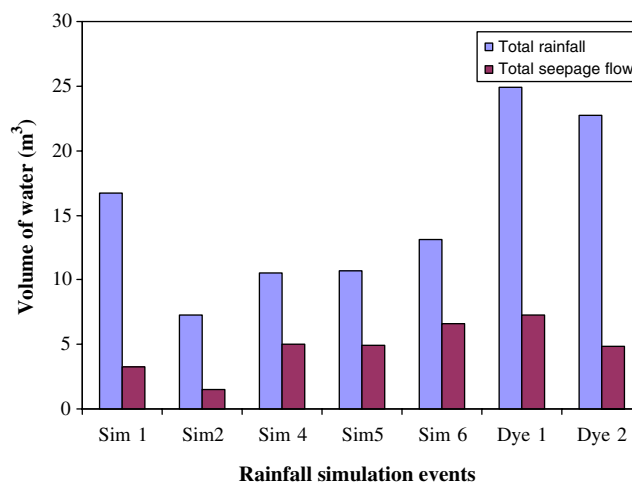


Fig. 10. Relationship between total seepage face flow and total rainfall from various rainfall simulations.

20 to 25 h for each rainfall simulation event as reflected in the TDR signals (Fig. 8). Thus, flow in such regions occurs not only through network of root channels and larger conduits but also through smaller fractures that are open as well as filled with mineral and organic materials. In other words, flow at the field site can be categorized into two distinct components including fast (preferential) flow through root channels and open fractures and slow (pseudo-matrix) flow through the fracture fills (clay layers and soil matrix).

Overall, subsurface flow in such juniper dominated karstic regions occurs essentially in a bimodal fashion, fast preferential/macropore flow and slow pseudo-matrix flow. The juniper roots play a major role in enhancing preferential flow in such regions as observed with our dye tracer studies discussed earlier. The smaller roots of juniper trees are conveniently located in the clay layers so that they have adequate water supply. Moreover, the larger roots accentuate the fractures by “wedging” or enlarging them. Several past studies (Newman et al., 1998, 2004; Wilcox et al., 1997; Wilcox, 2002) have clearly documented that roots enhance macropore flow. The fact that juniper enlarge fractures which in turn result in large volumes of subsurface flow makes the hydrology of such regions very complex from a hydrologic perspective and interesting from the water balance, and thus natural resources economics, perspective.

Another important observation during the rainfall simulations with high intensities was that the fracture fill clay layers started to wet up quickly. We observed that within 2 to 3 h from the start of the high intensity rainfall a significant portion of the clay lens was saturated. We believe that this is because of lateral water exchange process (different from pseudo-matrix flow discussed earlier) occurring between the matrix and macropore regions as observed in other controlled laboratory and numerical experiments (Köhne et al., 2004; Köhne and Mohanty, 2005). Also, this phenomenon was observed in the field by Newman et al. (1998, 2004) in their study of lateral subsurface flow in a ponderosa pine area in New Mexico. As the fracture fills receive water from the

adjacent root macropores due to lateral water transfer they become saturated and this saturated region grows with time.

CONCLUSIONS

Based on our experimental study in a juniper-covered plot underlain by karst geology with limestone bedrock virtually near the soil surface in Edwards plateau, Texas, fast subsurface flow was observed at various locations on the trench (seepage) face. Primarily, the fast (preferential) flow occurred through the fractures of the limestone units and through the juniper root channels. The responses at the trench face of the surface-applied water and dye tracers indicate that the well-developed channel network caused by juniper roots as well as geological fractures played a significant role in the proliferation of preferential flow processes. Flow rates were related to fracture size ranging from 0.00041 L s^{-1} at the tips of small roots to 0.5 L s^{-1} at the fractures of aperture $>10 \text{ mm}$. The simultaneous arrival of two different dyes applied at different distances from the trench face and near a tree base suggested that, after a lag time for initial wetting up and activation of flow paths, fast preferential flow dominated the vadose zone hydrology at the field site. Similar response times characterizing the onset of preferential flow at various locations in the trench face demonstrated recurrent flow patterns along similar flow paths for similar surface boundary conditions (rainfall intensity and amount).

Our results also indicated that preferential/macropore flow was primarily controlled by the imposed surface boundary conditions and was not significantly affected by initial moisture content of the profile. The flow network expands and contracts to accommodate varying rates of and amounts of water input. Slow pseudo-matrix flow that was registered by the TDR probes occurred through the fracture fills and matrix porosity. In many cases not all of the TDR sites responded to water inputs even after 20 to 30 h. On the basis of the sequence of various TDRs' responses and the irregular distribution of seepage locations across the trench face it can be inferred that flow at the field site is dominated by preferential flow through the channel network. The TDR responses revealed that during large rainfall events, there was significant lateral water exchange between the fractures and matrix porosity due to pressure difference across the two flow domains.

In summary, subsurface flow at the field site occurred as a combination of preferential/macropore flow and pseudo-matrix flow. Macropore flow occurred through root channels, natural karst fractures, and juniper root-enlarged fractures. Thus, it would seem justified that the presence of juniper trees would tend to decrease surface runoff as more water would infiltrate into the ground. However, our study is not spatially and temporally exhaustive enough to come up with an absolute answer to the complex and integrated ecohydrologic and hydrogeologic issues of such regions. Furthermore, such insights can only be validated when the entire water budget (streamflow, infiltration, interception, and ET) is quanti-

fied over an expansive spatiotemporal scale. Nevertheless, such a simplified and somewhat controlled ecohydrologic study provided us with an introductory knowledge about the nature, origin, and characteristics of hydraulic responses in the shallow subsurface of the Edwards Aquifer region with karst geology and juniper cover.

ACKNOWLEDGMENTS

This study was partially supported by a National Science Foundation (NSF) water cycle research (WCR) grant and a Texas Water Resources Institute (TWRI) equipment grant. We acknowledge the efforts of our collaborators Clyde Munster, Bradford Wilcox, Keith Owens, Geary Schindel, and several TAMU graduate students.

REFERENCES

- Archer, S. 1994. Woody plant encroachment into southwestern grasslands and savannas: Rates, patterns and proximate causes. p. 13–68. *In* M. Vavra et al. (ed.) Ecological implications of livestock herbivory in the west. Soc. for Range Manage., Denver, CO.
- ASTM. 1961. Methods for grain-size analysis of soils. ASTM Standards 4:1271–1283. ASTM, West Conshohocken, PA.
- Dugas, W.A., R.A. Hicks, and P. Wright. 1998. Effect of removal of *Juniperus ashei* on evapotranspiration and runoff in the Seco Creek Watershed. *Water Resour. Res.* 34:1499–1506.
- Flury, M., H. Flüher, W.A. Jury, and J. Leuenberger. 1994. Susceptibility of soils to preferential flow of water: A field study. *Water Resour. Res.* 30:1945–1954.
- Forrer, I., R. Kasteel, M. Flury, and H. Flüher. 1999. Longitudinal and lateral dispersion in an unsaturated field soil. *Water Resour. Res.* 35:3049–3060.
- Jardine, P.M., W.E. Sanford, J.P. Gwo, O.C. Reedy, D.S. Hicks, J.S. Riggs, and W.B. Bailey. 1999. Quantifying diffusive mass transfer in fractured shale bedrock. *Water Resour. Res.* 35:2015–2030.
- Käss, W. 1998. Tracing technique in geohydrology. A.A. Balkema, Rotterdam, The Netherlands.
- Kohne, J.M., B.P. Mohanty, J. Simunek, and H.H. Gerke. 2004. Numerical evaluation of a second-order water transfer term for variably-saturated dual permeability model. *Water Resources Res.* 40:W07409. doi:10.1029/2004WR003285.
- Kohne, B.P., and B.P. Mohanty. 2005. Water flow processes in a soil column with a cylindrical macropore: Experiment and hierarchical modeling. *Water Resour. Res.* 41:W03010. doi:10.1029/2004WR003303.
- Kuniansky, E.L., L. Fahlquist, and A.F. Ardis. 2001. Travel times along selected flow paths of the Edwards aquifer, Central Texas. USGS Water Resour. Invest. Rep. 01-4011:69–77. USGS, Denver, CO.
- McKay, L.D., J.A. Cherry, and R.W. Gillham. 1993. Field experiments in a fractured clay till. 2. Solute and colloid transport. *Water Resour. Res.* 29:3879–3890.
- McKay, L.D., J. Frederica, M. Lenczewski, J. Morthorst, and K.E.S. Klint. 1999. Spatial variability of contaminant transport in a fractured till, Avedore Denmark. *Nord. Hydrol.* 30:333–360.
- Mortensen, A.P., K.H. Jensen, B. Nilsson, and R.K. Juhler. 2004. Multiple tracing experiments in unsaturated fractured clayey till. Available at www.vadosezonejournal.org. *Vadose Zone J.* 3:634–644.
- Newman, B.D., A.R. Campbell, and B.P. Wilcox. 1998. Lateral subsurface flow pathways in a semiarid ponderosa pine hillslope. *Water Resour. Res.* 34:3485–3496.
- Newman, B.D., B.P. Wilcox, and R.C. Graham. 2004. Snowmelt-driven macropore flow and soil saturation in a semiarid forest. *Hydrol. Processes* 18:1035–1042.
- Richardson, C.W., E. Burnett, and R.W. Bovey. 1979. Hydrologic effects of brush control on Texas rangelands. *Trans. ASAE* 22:315–319.
- Side, R.C., B. Nilsson, M. Hansen, and J. Frederica. 1998. Spatially varying hydraulic and solute transport characteristics of a fractured till determined by field tracer tests, Funen, Denmark. *Water Resour. Res.* 34:2515–2527.
- Topp, G.C., J.L. Davis, and A.P. Annan. 1980. Electromagnetic determination of soil water content: Measurements in coaxial transmission lines. *Water Resour. Res.* 16:574–588.

- White, W.B. 1998. *Geomorphology and hydrology of Karst terrains*. Oxford Univ. Press, New York.
- White, W.B. 2002. Karst hydrology: Recent developments and open questions. *Eng. Geol.* 65:85–105.
- Wilcox, B.P. 2002. Shrub control and streamflow on rangelands: A process based viewpoint. *J. Range Manage.* 55:318–326.
- Wilcox, B.P., B.D. Newman, D. Brandes, D.W. Davenport, and K. Reid. 1977. Runoff from a semiarid ponderosa pine hillslope in New Mexico. *Water Resour. Res.* 33:2301–2314.
- Wright, H.A., F.M. Churchill, and W.C. Stevens. 1976. Effect of prescribed burning on sediment, water yield, and water quality from dozed juniper lands in central Texas. *J. Range Manage.* 29:294–298.